

Impacts of Midlatitude Western North Pacific Sea Surface Temperature Anomaly on the Subseasonal to Seasonal Tropical Cyclone Activity: Case Study of the 2018 Boreal Summer

Tomoe Nasuno¹, Masuo Nakano¹, Hiroyuki Murakami², Kazuyoshi Kikuchi², and Yohei Yamada¹

¹Japan Agency for Marine-Earth Science and Technology, Yokohama, Japan

²Geophysical Fluid Dynamics Laboratory, Princeton, NJ, USA

Abstract

In this study, we explored the impacts of midlatitude western North Pacific (WNP) sea surface temperature (SST) on tropical cyclone (TC) activity at intraseasonal to seasonal time scales during the 2018 boreal summer. During this period, a positive SST anomaly occurred in the midlatitude WNP and subtropical central Pacific; TC activity was abnormally high under the influence of the strong Asian summer monsoon. We performed sensitivity experiments using a global cloud system-resolving model for global SST (control, CTL) and SST that were regionally restored according to midlatitude WNP climatology (MWNPCLM). TC track density in the eastern WNP was higher in CTL than in MWNPCLM, in association with large-scale atmospheric responses; enhanced monsoon westerlies in the subtropical WNP, moist rising (dry subsiding) tendencies, and reduced (enhanced) vertical wind shear in the eastern (western) WNP. Enhanced TC activity in the eastern WNP was more distinct for intense TCs and during the active phase of intraseasonal oscillation (ISO). These results suggest that the impacts of midlatitude SST anomalies can reach lower latitudes to affect TC activity via large-scale atmospheric responses and ISO, which are usually overwhelmed by the impacts of SST anomalies in the tropics and subtropics.

(Citation: Nasuno, T., M. Nakano, H. Murakami, K. Kikuchi, and Y. Yamada, 2022: Impacts of midlatitude western North Pacific sea surface temperature anomaly on the subseasonal to seasonal tropical cyclone activity: Case study of the 2018 boreal summer. *SOLA*, **18**, 88–95, doi:10.2151/sola.2022-015.)

1. Introduction

Sea surface temperature anomalies (SSTAs) have major effects on the control of tropical cyclone (TC) activity. Over the western North Pacific (WNP), the primary impacts of the El Niño Southern Oscillation on the distribution and frequency of TCs and Asian summer monsoon have been extensively studied (Chan 1985; Wang and Chan 2002; Camargo and Sobel 2005; Yamada et al. 2019; Song et al. 2020; Takaya et al. 2021). For example, Asian summer monsoon and TC activity were successfully predicted for a period of > 1 year by simulating El Niño Southern Oscillation evolution and subsequent atmosphere–ocean variation (Takaya et al. 2021). Several recent studies have examined the prominent impacts of subtropical Pacific SSTA on TC activity (Zhang et al. 2016; Murakami et al. 2017; Qian et al. 2019; Takaya et al. 2019). High TC activity in 2018 was primarily related to high SSTA in the subtropical central Pacific, according to the results of sensitivity experiments using general circulation models (Qian et al. 2019). An unusually active summer monsoon in 2018 was mainly attributable to SSTA in the WNP, where midlatitude SSTA also play a role (Tseng et al. 2020). The impacts of midlatitude SSTA on TC activity have also been investigated by case studies of individual TCs that migrated into the midlatitudes (Kanada et al.

2017; Fujiwara and Kawamura 2021; Wada 2021). For example, warm SSTA over the Kuroshio current remotely affected the development of TC Chaba in 2010 through enhanced moisture transport and latent heat flux, as determined in short-term (5 days) experiments using a regional atmospheric model (Fujiwara and Kawamura 2021); general insights require further case studies because of variation among individual TCs at short time scales.

At subseasonal to seasonal time scales, WNP TC activity is highly modulated by intraseasonal oscillation (ISO) and variability in Asian summer monsoon (Yoshida et al. 2014; Nakano et al. 2015, 2021; Camargo et al. 2009; Fowler and Pritchard 2020; Qian et al. 2020; Kikuchi 2021; Lee et al. 2013; Nasuno et al. 2016). These studies have indicated enhanced TC activity during the active ISO period through modifications of large-scale dynamical and thermodynamical fields. However, the extent to which SSTAs in the tropics, subtropics, and midlatitudes affect WNP TC activity at subseasonal time scales (and associated seasonal time scales) remains unclear. Therefore, the objective of this study was to fill the knowledge gap that exists between basin-scale interannual TC activity studies and individual midlatitude TC case studies. In particular, there is a need to determine whether and to what extent recent significant SSTAs in the midlatitudes (e.g., Hayashi et al. 2021) significantly impact WNP TC activity. We conducted a suite of sensitivity experiments using a global cloud-system-resolving model to explore the seasonal TC activity and large-scale atmospheric responses to midlatitude WNP SSTA, as well as their association with ISO during the 2018 boreal summer.

2. Boreal summer in 2018

During the boreal summer (July–September) of 2018, a positive SSTA occurred over the midlatitude WNP, subtropical central Pacific (partly caused by the Pacific Meridional Mode; Chiang and Vimont 2004), and tropical central to eastern Pacific. In contrast, SSTA was neutral or weakly negative over the South China Sea and Philippine Sea (Fig. 1a). Accordingly, the upward Walker circulation branch shifted eastward compared with the climatology (Fig. S1), consistent with the eastward extension of lower tropospheric westerly anomalies (i.e., monsoon trough) and with the presence of anomalous convective activity over the tropical Pacific (Fig. 1c), indicating strong Asian summer monsoon. Under these conditions, TCs tended to develop in the eastern WNP and central Pacific (Fig. 1e). Robust ISO signals occurred repeatedly in summer, and TC genesis occurred selectively during their active periods (Fig. S2).

3. Method and data

3.1 Design of sensitivity experiments

We used Nonhydrostatic Icosahedral Atmospheric Model (NICAM; Satoh et al. 2014) in sensitivity experiments to investigate the impacts of the midlatitude WNP SSTA on TC activity. We used a horizontal mesh size of 14 km globally, which marginally represents TC structure (Yamada et al. 2017), and 38 vertical levels with a top height of 40 km. Moist convection was explicitly rep-

Corresponding author: Tomoe Nasuno, Japan Agency for Marine-Earth Science and Technology, 3173-25, Showa-machi, Kanazawa-ku, Yokohama, 236-0001, Kanagawa, Japan. E-mail: nasuno@jamstec.go.jp.



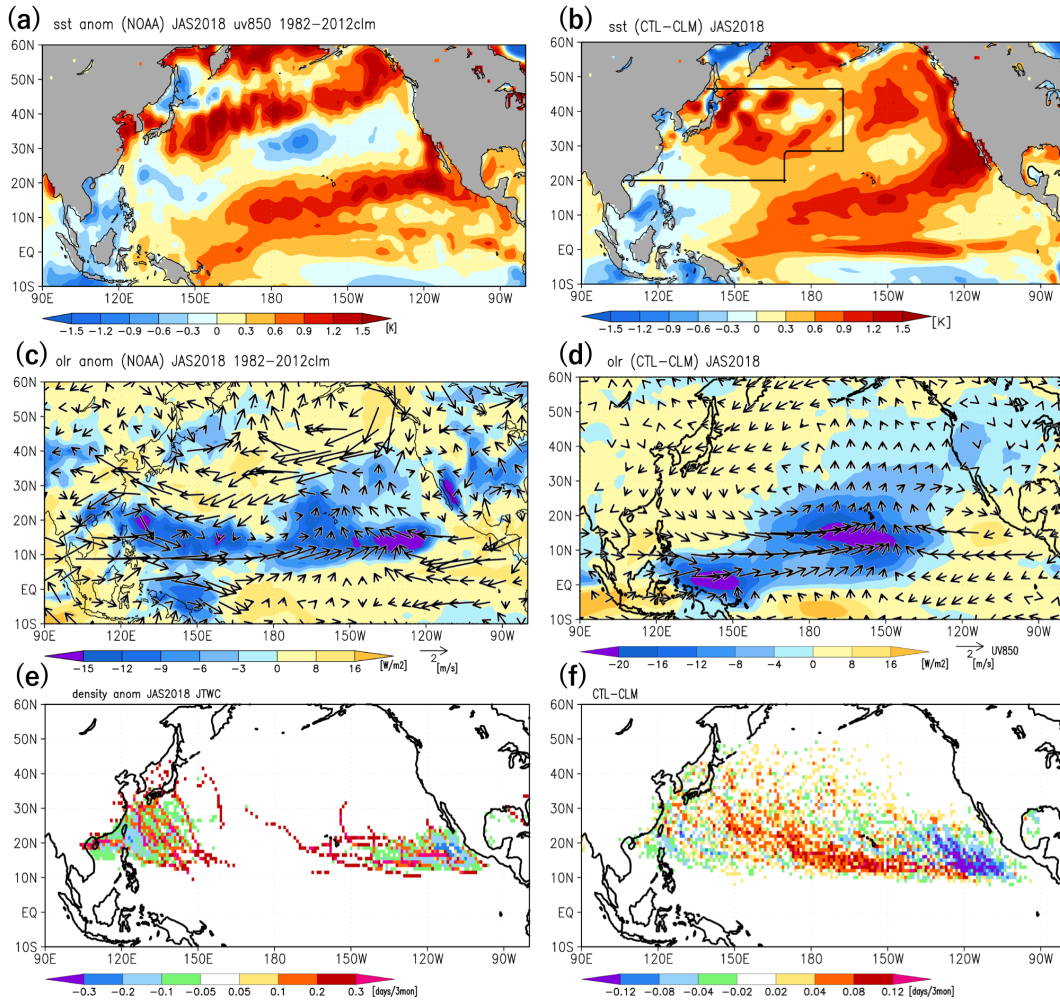


Fig. 1. (a) National Oceanic and Atmospheric Administration (NOAA) Optimum Interpolation Sea Surface Temperature (OISST), (c) Anomalous NOAA Outgoing Longwave Radiation (OLR) data with 850-hPa wind vectors in the Japanese 55-year Reanalysis product (JRA-55), and (e) Anomalous tropical cyclone (TC) track density for the Joint Typhoon Warning Center best track during July–September 2018. Anomalies are defined as deviations from climatology (averaged for 1982–2012, 1979–2010, and 1980–2018 for the NOAA OISST/JRA-55, NOAA OLR, and best track products, respectively). (b, d, f) As in (a, c, e), but for an ensemble mean of CTL simulations [deviations from SSTs restored to climatology (CLM)]. Box in (b) indicates the midlatitude WNP domain, in which SSTA values were replaced with zero in MWNPCML simulations.

resented using a cloud microphysics scheme (Tomita 2008; Roh and Satoh 2014) without a cumulus parameterization scheme. At the bottom boundary, SST was predicted using a slab ocean model with a 15-m mixed layer depth, and the predicted SST was nudged to the prescribed time-series SST at a relaxation time of 7 days.

The sensitivity experiments were designed in accordance with the method used by Qian et al. (2019)¹, which examined SSTA impacts on TCs by restoring the Pacific regional SSTs to the climatology using the Geophysical Fluid Dynamics Laboratory Forecast-oriented Low Ocean Resolution (FLOR) global coupled model (Vecchi et al. 2014). In the first set of experiments, global SSTs in 2018 were used as nudging data (CTL; Fig. 1b), whereas in the second set, we used SSTs that had been restored to the climatology (1982–2012) over the midlatitude WNP (MWNPCML; Fig. 1b). As a reference, we also conducted experiments in which SSTs were restored to the climatology. We nudged the simulated SSTs to the Qian et al. (2019) SST time series, which consists of 12-member ensembles for each setting, rather than observed SSTs, to confirm the robustness of the results with slight changes in the SSTA distributions. The simulation target period was July–September 2018, and the initial atmospheric data were interpo-

lated from the Japanese 55-year Reanalysis product (JRA-55; Kobayashi et al. 2015). For each SST setting, 36-member ensemble experiments were conducted (Supplement 3); thus, we mainly present the 36-member period-mean results in this study.

For real-world comparison, we used the JRA-55, National Oceanic and Atmospheric Administration (NOAA) Interpolated Outgoing Longwave Radiation (OLR) (Liebmann and Smith 1996), NOAA Optimum Interpolation Sea Surface Temperature (OISST) (Huang et al. 2021), and International Best Track Archive for Climate Stewardship (IBTrACS; Knapp et al. 2010) datasets.

3.2 Analysis method

a. TC tracking

We applied TC tracking methods described in previous studies (Nakano et al. 2015; Yamada et al. 2017) to 6-hourly simulation outputs. TC candidates were detected and traced for a minimum pressure. TCs were extracted in accordance with the following criteria: maximum 10-m wind speed ($> 17.5 \text{ m s}^{-1}$), 850-hPa vorticity, warm core structure, and duration ($> 36\text{-h}$). TC genesis and track density were counted on a $1^\circ \times 1^\circ$ grid.

b. ISO composite

In this study, we defined the ISO according to band-pass-filtered convective anomalies averaged at 115°E – 160°E that per-

¹ Our simulation dataset includes 12-member NICAM simulation data from Qian et al. (2019).

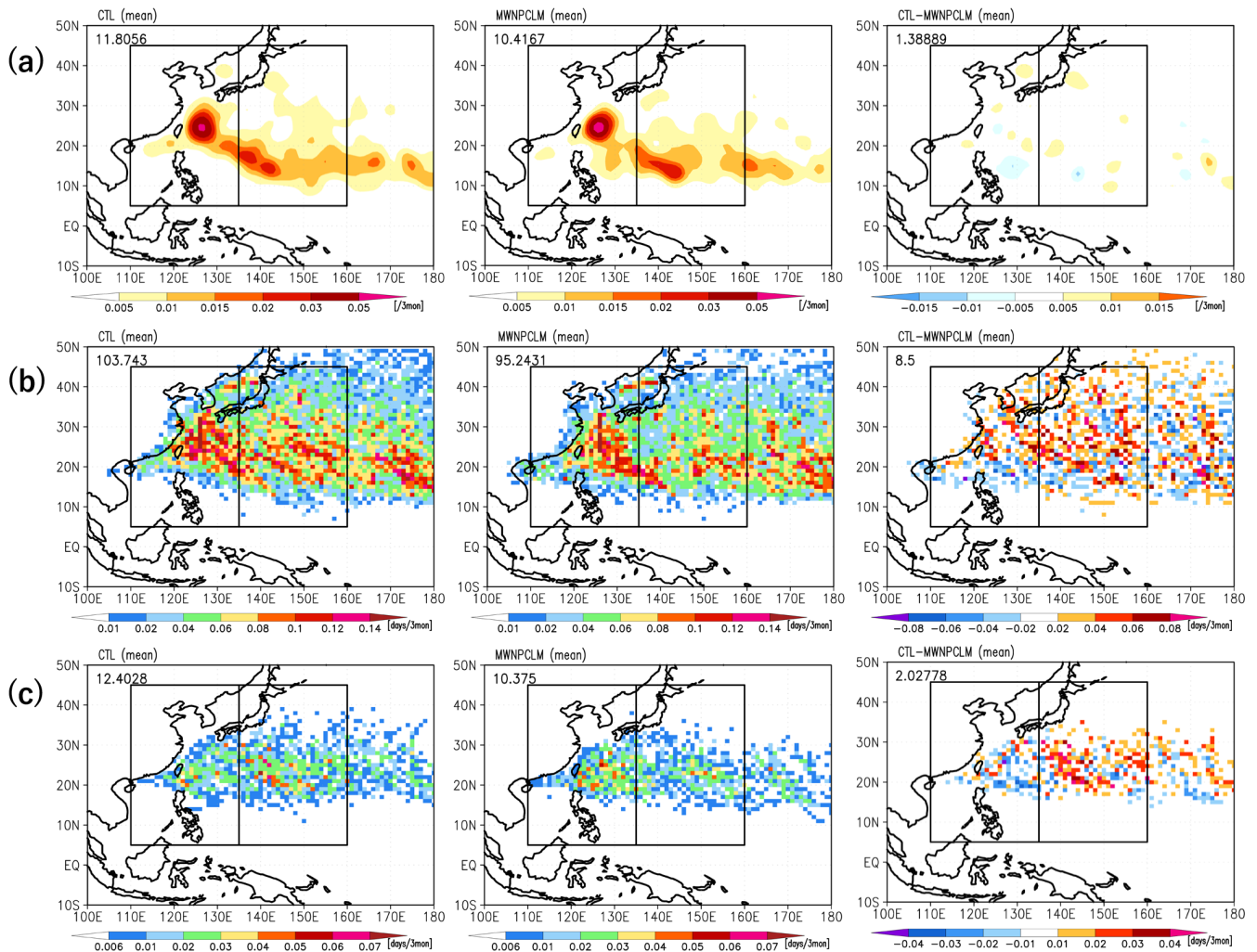


Fig. 2. Horizontal distribution of 3-month accumulated (a) TC genesis, (b) TC track density, and (c) TC track density at maximum 10-m wind speed $> 45 \text{ m s}^{-1}$ in CTL (left panels), MWNPCLM (center panels), and their difference (CTL-MWNPCLM) (right panels). Numbers in the upper-left corner of each panel are sums over the plot area. Horizontal smoothing was performed for (a).

sisted for longer than 10 days and continuously propagated northward (Supplement 2). This simple method extracts the ISO signals in the observed OLR (Fig. S2); it is sufficient for the purposes of this study. The ISO events with a minimum OLR anomaly of 1.1 standard deviations were used for composite analysis (64 events per simulation case), where the base point was defined as the date of the minimum OLR anomaly in each event.

4. Results

The period-mean fields of CTL (Figs. 1b and 1d) reproduced enhanced convective activity in the broad domain over the tropical and subtropical western to central Pacific, which was associated with lower tropospheric westerly anomalies intruding into the central Pacific. These anomalies represent the active Asian summer monsoon, although some biases were detected near the Philippine Sea and in higher-latitude wind anomalies. This enhanced convection in the central Pacific closely corresponded with the warm SSTA in that region. The anomalous positive (negative) TC track density in the eastern (western) WNP reproduced the observed characteristics (Figs. 1e and 1f).

4.1 Period-mean TC responses in the WNP

The horizontal distribution of accumulated TC genesis and track density in CTL and MWNPCLM in the WNP domain are

shown in Fig. 2. The accumulated track density over the plot area was 103.7 days for CTL, which was similar to the accumulated track density for the observed data (105.5 days), with a bias of fewer generated TCs (12) than in the observed data (19).

Next, we focused on SSTA impacts by evaluating differences between CTL and MWNPCLM. Both TC genesis and track density were greater in CTL than in MWNPCLM, by 10% and 8.2%, respectively (Figs. 2a and 2b). We detected distinct differences in track density in the eastern WNP, particularly to the south of the SSTA modification (25°N – 35°N , 130°E – 165°E) (Fig. 2b). The regional difference in track density was more evident for intense TCs (with maximum wind speed $> 45 \text{ m s}^{-1}$) (Fig. 2c, Table 1) with peak TC density near 140°E (120°E) in CTL (MWNPCLM). These domains of the substantial changes in track density did not exactly coincide with the domain of the SSTA change, suggesting a substantial remote effect of the SSTA on large-scale circulation. Difference in TC genesis distributions was unclear (Fig. 2a), implying that TC path and development changes were the major cause of differences in TC track density.

To understand how the midlatitude WNP SSTA caused these TC activity changes, we examined the atmospheric responses (CTL-MWNPCLM) relevant to the TC genesis environment (Fig. 3). All of these responses exhibited more (less) favorable conditions for TC activity in the subtropical eastern (western) WNP (15°N – 25°N , 140°E – 170°E) [15°N – 25°N , 115°E – 130°E] in CTL than in MWNPCLM. As a response to the warm SSTA

Table 1. Impacts of midlatitude western North Pacific (WNP) sea surface temperature anomalies (SSTA) and intraseasonal oscillation (ISO) on tropical cyclone (TC) track density (%) for the western (5°N–45°N, 110°E–135°E), eastern (5°N–45°N, 135°E–160°E), and total (0°N–49°N, 100°E–180°E) WNP. Bold numbers indicate > 90% significance levels. Impacts were assessed by (CTL – MWNPCML)/CTL [(ISO active – period-mean)/period-mean] for midlatitude WNP SSTA (ISO).

	TC_all			TC ($V_{max} > 45 \text{ m s}^{-1}$)		
	west	east	all	west	east	all
MWNP SSTA impact						
mean	1.82	15.77	8.19	-37.62	34.42	16.34
ISO active	-7.67	23.82	7.73	-31.34	70.93	32.96
ISO impact						
CTL	53.15	13.2	14.07	120.97	65.32	64.64
MWNPCLM	67.95	2.38	14.64	110.89	-26.71	31.94

in the midlatitude WNP, positive temperature (negative pressure) anomaly was formed in the lower troposphere (Figs. S4d, S4f, and S4h), and anomalous cyclonic circulation appeared through geostrophic balance (Fig. S4g). The wind anomaly extended to the south of the SSTA region, with enhanced lower tropospheric convergence and westerly anomalies toward the central Pacific anomalous convective region (Figs. 1d and 3a). Enhanced westerlies (easterlies) in the lower (upper) troposphere (Figs. S4a and S4c) resulted in decreased (increased) vertical shear in the subtropical (tropical) WNP (Fig. 3b). Ascending southerly (descending northerly) anomalies in the eastern (western) WNP advected moist (dry) air from lower-latitude (higher-latitude) areas (Figs. 3c and 3d), consistent with the enhanced (suppressed) convection (Fig. 3a) and TC density (Figs. 2b and 2c) in these regions. The steering wind (mass-weighted vertical average of horizontal wind) was also altered accordingly, explaining the more northerly trend of the TC path in the eastern WNP in CTL than in MWNPCLM (Figs. 2b, 2c and 3d).

4.2 Modulation of TC responses by ISO

The composite TC track density during the active phase (peak 10 days) of the ISO (converted to 3-month accumulations) is shown in Fig. 4. Both CTL and MWNPCLM showed a > 10% increase in accumulated track density in the WNP, with greater concentration toward the south (< 25°N; Figs. 4a and 4b); these findings were consistent with observed impacts of ISO phase on TC track density (Nakano et al. 2021; Hirata and Kawamura 2014). In MWNPCLM, zonal contrast in the period-mean distribution (Fig. 2b) was exaggerated during the active ISO phase (Fig. 4b). Track density sums for the subdomains of the WNP during the active phase of the ISO and during July–September are shown in Fig. 5a. The increase in track density during the active ISO phase was more pronounced in the western WNP than in the eastern WNP (Fig. 5a).

For intense TCs, the impact of the ISO phase on TC activity was greater (Figs. 4c, 4d, 5b, and Table 1). The increases in TC track density during the active ISO phase for CTL and MWNPCLM were 65% and 32% of the period-mean values, respectively (Table 1). In CTL, the increase caused by the ISO broadly appeared in the subtropical WNP, over both the western and eastern subdomains (Fig. 4d). In contrast, the increase caused by the ISO (over the period-mean value) was greater in MWNPCLM than in CTL in the western subdomain of the WNP, whereas a deficit was detected in the eastern subdomain (Fig. 5b). Thus, the impacts of the ISO phase on TC track density showed distinct regional differences among intense TCs in MWNPCLM.

To determine the causes of these TC activity responses to the ISO with and without the SSTA in the midlatitude WNP, we examined the anomalous TC genesis environment (ISO active phase–period-mean values) for both cases (Fig. 6). The peak of anomalous convective activity was located near 5°N–15°N, 120°E–150°E, which was consistent with the definition of the ISO adopted in this study (Fig. 6a). A large-scale cyclonic circulation formed to the northwest of the convective peak (10°N–25°N, 105°E–135°E), as typically observed in the active period of the boreal summer ISO (Guo et al. 2021; Kikuchi 2021; Lee et al. 2013). To the north (20°N–35°N, 130°E–155°E), anticyclonic circulation appeared with suppressed convection as a remote

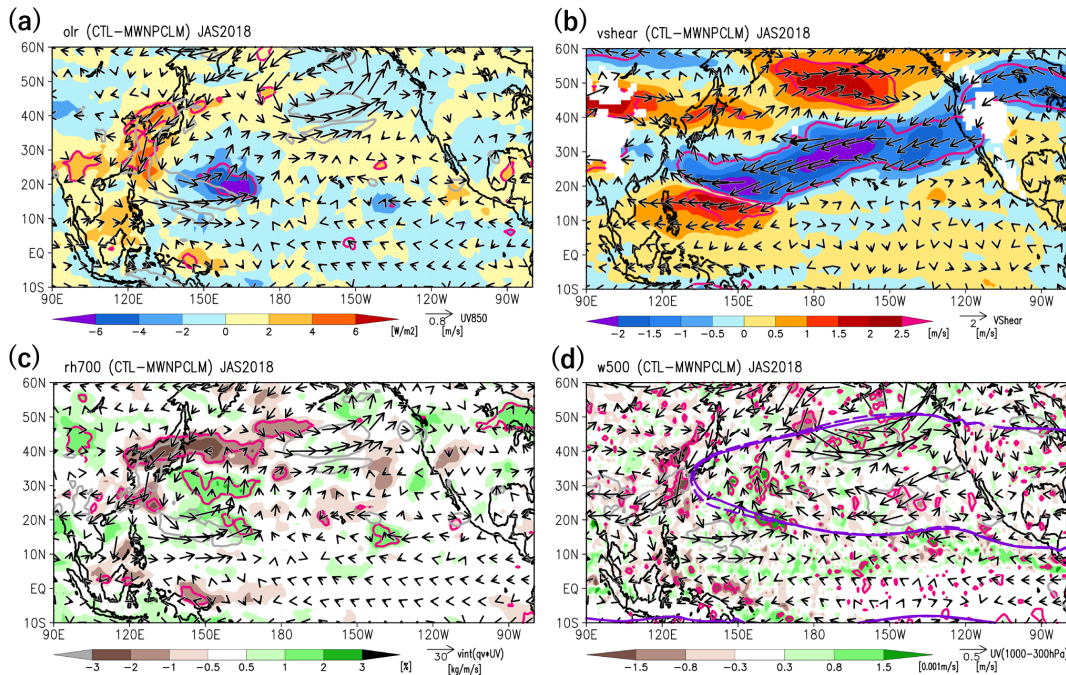


Fig. 3. Period-mean (July–September 2018) responses (CTL–MWNPCLM) of (a) OLR and 850-hPa wind vectors, (b) vertical shear of zonal wind (difference between 200 and 850 hPa) and shear vector, (c) 700-hPa relative humidity and vertically integrated moisture flux, and (d) 500-hPa vertical velocity and mass-weighted 300–1,000-hPa integral of zonal wind vectors. Purple contour lines in (d) indicate an 850-hPa geopotential height of 1,520 gpm in CTL (solid line) and MWNPCLM (dashed line). Magenta (gray) contour lines indicate the 90% significance level for shading (vectors).

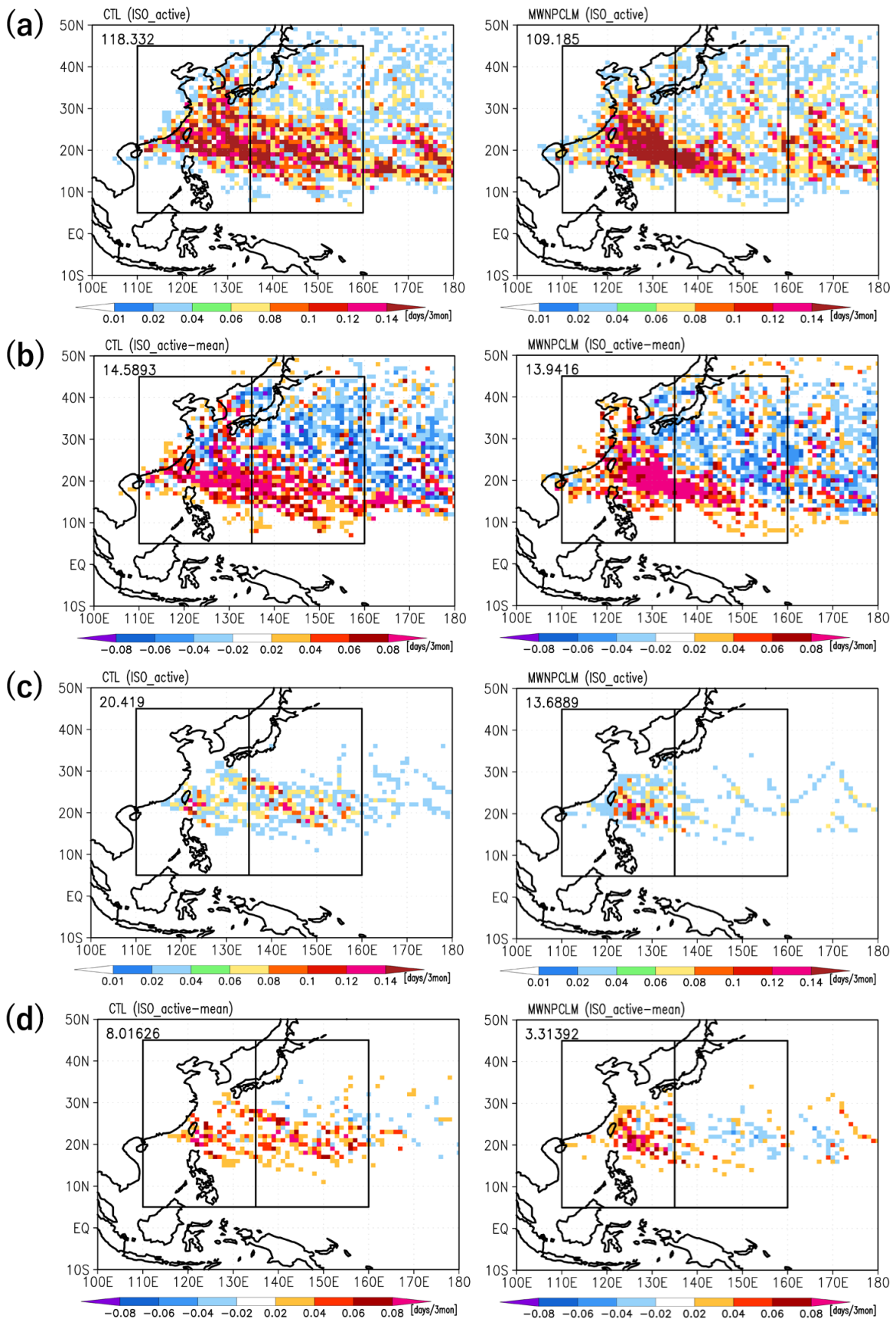


Fig. 4. Horizontal distribution of composite (a) TC track density in the active intraseasonal oscillation (ISO) phase. (b) As in (a), but for deviations from the period-mean in CTL (left panels) and MWNPCLM (right panels). (c, d) As in (a, b), but for TCs with maximum 10-m wind speed $> 45 \text{ m s}^{-1}$. Numbers in the upper-left corner of each panel are summed over the plot area. TC track density values for the active ISO phase (peak 10 days) were converted to a 3-month accumulated value.

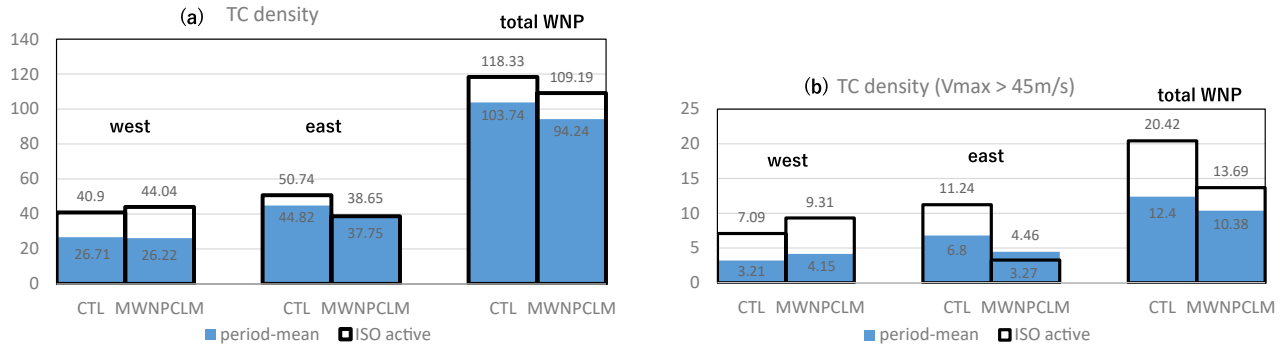


Fig. 5 Box plot of (a) TC track density in the (left) western (5°N–45°N, 110°E–135°E), (center) eastern (5°N–45°N, 135°E–160°E), and (right) total (0°N–49°N, 100°E–180°E) WNP for the ISO active phase (black box) and period-mean (blue box) in CTL (left columns) and MWNPCML (right columns). TC track density values for the ISO active phase (peak 10 days) were converted to a 3-month accumulated value.

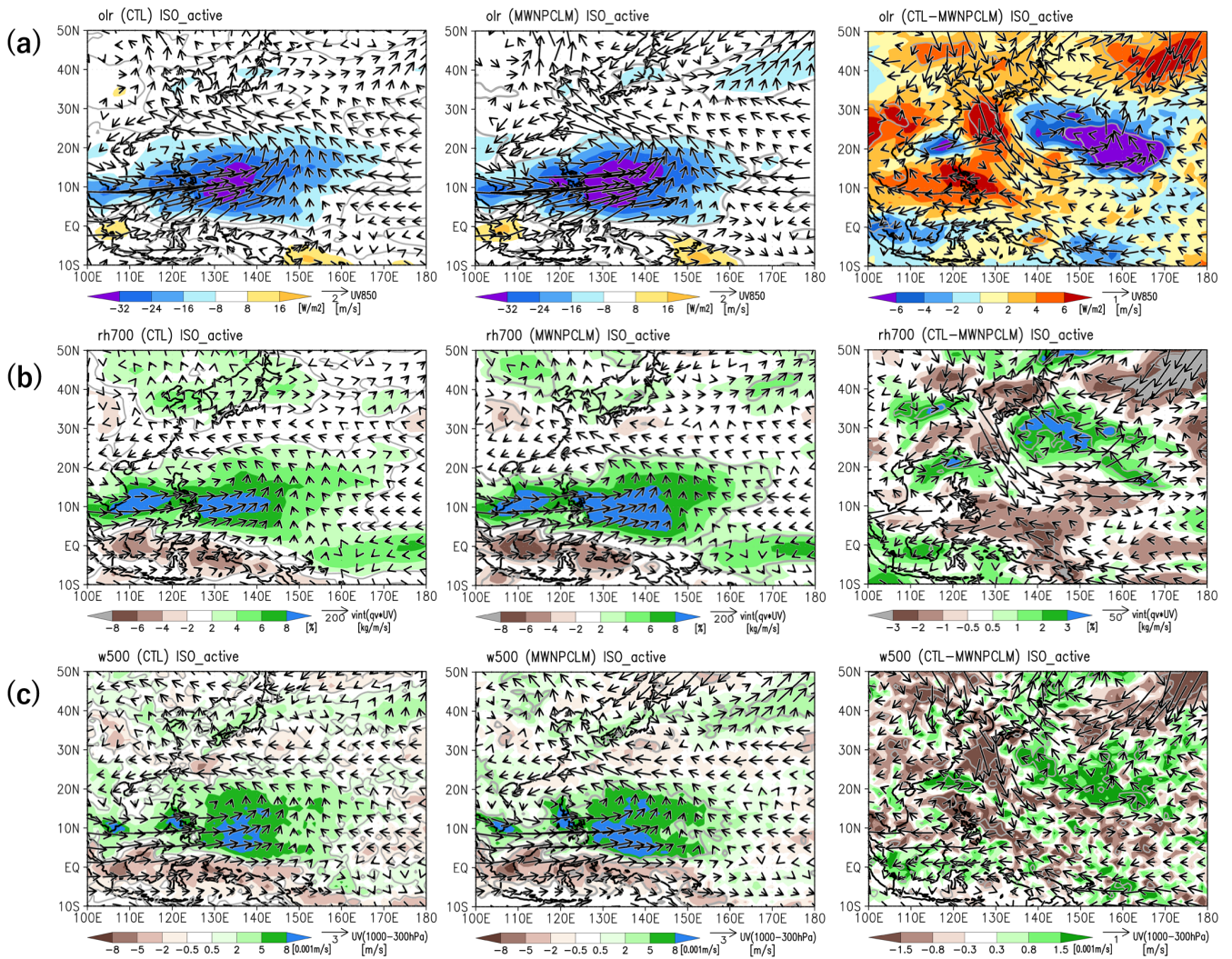


Fig. 6 Composite of the ISO active phase (deviations from period-mean values) (a) OLR and 850-hPa horizontal wind vectors, (b) 700-hPa relative humidity and vertically integrated moisture flux, and (c) 500-hPa vertical velocity and mass-weighted 300–1,000-hPa integral of zonal wind vectors in CTL (left panels) and MWNPCML (center panels). The difference (CTL–MWNPCML) during the ISO active phase is also plotted (right panels). Gray contour lines indicate a 90% significance level.

response to tropical convective activity. Both positive and negative anomalies were more pronounced in MWNPCML than in CTL (Fig. 6a). Consistent with the enhanced convective activity, anomalous moistening formed in the middle troposphere, along with northwestward moisture flux (Fig. 6b) and enhanced upward

motion (Fig. 6c); these changes created favorable conditions for TC genesis and development, thus explaining the simulated enhancement of TC activity in both cases in the southwestern WNP. These findings are consistent with previous conclusions based on long-term ISO analyses (Moon et al. 2018; Fowler and Pritchard

2020). In addition, vertical wind shear becomes unfavorable for TC activity and development because of enhanced easterly shear associated with the ISO. We interpret the greater increase in upward motion in the western subdomain of the WNP in MWNPCML than in CTL as a major cause of the marked increase in strong TCs in this region (Fig. 6, right panels), whereas TC track density increased even in the eastern WNP in CTL. Both of these factors may be associated with the period-mean state difference detected in this study.

5. Conclusions

In this study, sensitivity experiments conducted using a global cloud-system resolving model demonstrated that the midlatitude WNP SSTA observed during the 2018 boreal summer systematically affected TC activity and particularly distribution within the WNP via large-scale atmospheric response and modulation associated with the ISO (Table 1). Under the 2018 summer conditions with strong Asian summer monsoon, the midlatitude WNP SSTA contributed to increased TC track density in the eastern WNP, by 16% for July–September and 24% for the active ISO phase, through the enhancement of cyclonic circulation in the WNP, an associated moist upward tendency, and reduced vertical wind shear. During the active ISO phase, TC track density was commonly increased in the western WNP, while increased TC track density occurred in the eastern WNP (by 65%) only under the positive midlatitude WNP SSTA. This contrast between the western and eastern subdomains of the WNP was more pronounced for intense TCs, suggesting high sensitivity of TC intensification to the environment.

The impacts of the midlatitude SSTA on WNP TC track density were regarded as secondary to subtropical or tropical SSTA impacts (Qian et al. 2019, Supporting Text S3, Fig. S8; Tseng et al. 2020). Our results suggest that the midlatitude SSTA affected the lower latitudes in some cases: in summer 2018, over a humid subtropical central Pacific, meridional and zonal contrasts in climatological convection and circulation were relaxed; this may have enhanced the atmospheric response to the midlatitude SSTA, thereby reaching the lower latitudes. Future studies should investigate the impacts of midlatitude SSTAs under various background conditions.

In this study, we represented air–sea interactions in a simple manner. Using an atmospheric general circulation model, Ohba and Ueda (2006) obtained cyclonic circulation responses to a positive SSTA over the WNP in June through local convective instability and sea level pressure deficit, consistent with the atmospheric response to the midlatitude WNP SSTA in this study, as well as Tseng et al.'s (2020) results. The role of air–sea interactions is another topic that requires further investigation.

Acknowledgements

T. Nasuno is supported by JSPS KAKENHI Grant Number JP20H05172, JP19H04248, and JP20H01386. M. Nakano is supported by JSPS KAKENHI Grant Number JP20H05175. The NICAM simulations are conducted on K computer (proposal number: hp180182) and on the Earth Simulator in JAMSTEC, and post processed on the Data Analyzer at JAMSTEC. We thank Japan Meteorological Agency for providing the JRA-55 data, the National Oceanic and Atmospheric Administration, Physical Sciences Laboratory (PSL), NOAA for providing the Interpolated OLR and the NOAA OI SST V2 data, and National Climatic Data Center (NCDC), NOAA for providing TBTrACS.

Edited by: A. Manda

Supplement

Supplement 1 shows the anomalous Walker circulation in 2018. Supplement 2 describes the definition of the ISO in this study. Supplement 3 describes the details of the ensemble simulations. Supplement 4 describes the details of the atmospheric responses to the SSTA. Supplement 5 describes sensitivity to the subtropical WNP SSTA.

References

- Camargo, S. J., and A. H. Sobel, 2005: Western North Pacific tropical cyclone intensity and ENSO. *J. Climate*, **18**, 2996–3006, doi:10.1175/JCLI3457.1.
- Camargo, S. J., M. C. Wheeler, and A. H. Sobel, 2009: Diagnosis of the MJO modulation of tropical cyclogenesis using an empirical index. *J. Atmos. Sci.*, **66**, 3061–3074.
- Chan, J. L., 1985: Tropical cyclone activity in the northwest Pacific in relation to the El Niño/Southern Oscillation phenomenon. *Mon. Wea. Rev.*, **113**, 599–606.
- Chiang, J. C. H., and D. J. Vimont, 2004: Analogous Pacific and Atlantic meridional modes of tropical atmosphere-ocean variability. *J. Climate*, **17**, 4143–4158, doi:10.1175/JCLI4953.1.
- Fowler, M. D., and M. S. Pritchard, 2020: Regional MJO modulation of northwest Pacific tropical cyclones driven by multiple transient controls. *Geophys. Res. Lett.*, **47**, e2020GL087148.
- Fujiwara, K., and R. Kawamura, 2021: Active role of sea surface temperature changes over the Kuroshio in the development of distant tropical cyclones in boreal fall. *J. Geophys. Res. Atmos.*, **126**, e2021JD035056.
- Guo, X., N. Zhao, K. Kikuchi, T. Nasuno, M. Nakano, and H. Annamalai, 2021: Atmospheric rivers over the Indo-Pacific and its associations with boreal summer intraseasonal oscillation. *J. Climate*, doi:10.1175/JCLI-D-21-0290.1 (in press).
- Hayashi, M., H. Shiogama, S. Emori, T. Ogura, and N. Hirota, 2021: The northwestern Pacific warming record in August 2020 occurred under anthropogenic forcing. *Geophys. Res. Lett.*, **48**, e2020GL090956.
- Hirata, H., and R. Kawamura, 2014: Scale interaction between typhoons and the North Pacific subtropical high and associated remote effects during the Baiu/Meiyu season. *J. Geophys. Res. Atmos.*, **119**, 5157–5170, doi:10.1002/2013JD021430.
- Huang, B., C. Liu, V. Banzon, E. Freeman, G. Graham, B. Hankins, T. Smith, and H.-M. Zhang, 2021: Improvements of the Daily Optimum Interpolation Sea Surface Temperature (DOISST) Version 2.1. *J. Climate*, **34**, 2923–2939, doi:10.1175/JCLI-D-20-0166.1.
- Kanada, S., S. Tsujino, H. Aiki, M. K. Yoshioka, Y. Miyazawa, K. Tsuboki, and I. Takayabu, 2017: Impacts of SST patterns on rapid intensification of Typhoon Megi (2010). *J. Geophys. Res. Atmos.*, **122**, 13245–13262, doi:10.1002/2017JD027252.
- Kikuchi, K., 2021: The boreal summer intraseasonal oscillation (BSISO): A review. *J. Meteor. Soc. Japan*, **99**, 933–972, doi:10.2151/jmsj.2021-045.
- Knapp, K. R., D. H. Levinson, H. J. Diamond, and C. J. Neumann, 2010: The International Best Track Archive for Climate Stewardship (IBTrACS): Unifying tropical cyclone data. *Bull. Amer. Meteor. Soc.*, **91**, 363–376.
- Kobayashi, S., Y. Ota, Y. Harada, A. Ebata, M. Moriya, H. Onoda, K. Onogi, H. Kamahori, C. Kobayashi, H. Endo, K. Miyazaki, and K. Takahashi, 2015: The JRA-55 reanalysis: General specifications and basic characteristics. *J. Meteor. Soc. Japan*, **93**, 5–48, doi:10.2151/jmsj.2015-001.
- Lee, J.-Y., B. Wang, M. C. Wheeler, X. Fu, D. E. Waliser, and I.-S. Kang, 2013: Real-time multivariate indices for the boreal summer intraseasonal oscillation over the Asian summer monsoon region. *Climate Dyn.*, **40**, 493–509.

- Liebmann, B., and C. A. Smith, 1996: Description of a complete (interpolated) outgoing longwave radiation dataset. *Bull. Amer. Meteor. Soc.*, **77**, 1275–1277.
- Moon, J.-Y., B. Wang, S.-S. Lee, and K.-J. Ha, 2018: An intraseasonal genesis potential index for tropical cyclones during Northern Hemisphere summer. *J. Climate*, **31**, 9055–9071.
- Murakami, H., G. A. Vecchi, T. L. Delworth, A. T. Wittenberg, S. Underwood, R. Gudgel, and co-authors, 2017: Dominant role of subtropical Pacific warming in extreme eastern Pacific hurricane seasons: 2015 and the future. *J. Climate*, **30**, 243–264.
- Nakano, M., M. Sawada, T. Nasuno, and M. Satoh, 2015: Intraseasonal variability and tropical cyclogenesis in the western North Pacific simulated by a global nonhydrostatic atmospheric model. *Geophys. Res. Lett.*, **42**, 565–571.
- Nakano, M., F. Vitart, and K. Kikuchi, 2021: Impact of the boreal summer intraseasonal oscillation on typhoon tracks in the western North Pacific and the prediction skill of the ECMWF model. *Geophys. Res. Lett.*, **48**, e2020GL091505, doi:10.1029/2020GL091505.
- Nasuno, T., H. Yamada, M. Nakano, H. Kubota, M. Sawada, and R. Yoshida, 2016: Global cloud-permitting simulations of Typhoon Fengshen (2008). *Geophys. Res. Lett.*, **3**, doi:10.1186/s40562-016-0064-1.
- Ohba, M., and H. Ueda, 2006: A role of zonal gradient of SST between the Indian Ocean and the Western Pacific in localized convection around the Philippines. *Atmosphere*, **2**, 176–179.
- Qian, Y., H. Murakami, M. Nakano, P.-C. Hsu, T. L. Delworth, S. B. Kapnick, V. Rammawamy, T. Mochizuki, Y. Morioka, T. Doi, T. Kataoka, T. Nasuno, and K. Yoshida, 2019: On the mechanisms of the active 2018 tropical cyclone season in the North Pacific. *Geophys. Res. Lett.*, **46**, 12293–12302.
- Qian, Y., P.-C. Hsu, H. Murakami, B. Xiang, and L. You, 2020: A hybrid dynamical-statistical model that advances the sub-seasonal tropical cyclone prediction over the western North Pacific. *Geophys. Res. Lett.*, **47**, e2020GL090095.
- Roh, W., and M. Satoh, 2014: Evaluation of precipitating hydrometeor parameterizations in a single-moment bulk microphysics scheme for deep convective systems over the Tropical Central Pacific. *J. Atmos. Sci.*, **71**, 2654–2673.
- Satoh, M., H. Tomita, H. Yashiro, H. Miura, C. Kodama, T. Seiki, A. T. Noda, Y. Yamada, D. Goto, M. Sawada, T. Miyoshi, Y. Niwa, M. Hara, Y. Ohno, S. Iga, T. Arakawa, T. Inoue, and H. Kubokawa, 2014: The Non-hydrostatic icosahedral atmospheric model: Description and development. *Prog. Earth Planet. Sci.*, **1**, 18.
- Song, J., P. J. Klotzbach, and Y. Duan, 2020: Differences in western North Pacific tropical cyclone activity among three El Niño phases. *J. Climate*, **33**, 7983–8002, doi:10.1175/JCLI-D-20-0162.1.
- Takaya, Y., 2019: Positive phase of Pacific meridional mode enhanced western North Pacific tropical cyclone activity in summer 2018. *SOLA*, **15A**, 55–59.
- Takaya, Y., Y. Kosaka, M. Watanabe, and S. Maeda, 2021: Skillful predictions of the Asian summer monsoon one year ahead. *Nature Commun.*, **12**, 2094, doi:10.1038/s41467-021-22299-6.
- Tseng, W.-L., C.-C. Hong, M.-Y. Lee, H.-H. Hsu, and C.-C. Chang, 2020: Compound effect of local and remote sea surface temperature on the unusual 2018 western North Pacific summer monsoon. *J. Meteor. Soc. Japan*, **98**, 1369–1385.
- Tomita, H., 2008: New microphysics with five and six categories with diagnostic generation of cloud ice. *J. Meteor. Soc. Japan*, **86A**, 121–142.
- Vecchi, G. A., T. Delworth, R. Gudgel, S. Kapnick, A. Rosati, A. T. Wittenberg, and co-authors, 2014: On the seasonal forecasting of regional tropical cyclone activity. *J. Climate*, **27**, 7994–8016, doi:10.1175/JCLI-D-14-00158.1.
- Yamada, Y., M. Satoh, M. Sugi, C. Kodama, A. T. Noda, M. Nakano, and T. Nasuno, 2017: Response of tropical cyclone activity and structure to global warming in a high-resolution global nonhydrostatic model. *J. Climate*, **30**, 9703–9724, doi:10.1175/JCLI-D-17-0068.1.
- Yamada, Y., C. Kodama, M. Satoh, M. Nakano, T. Nasuno, and M. Sugi, 2019: High-resolution, ensemble simulations of intense tropical cyclones and their internal variability during the El Niños of 1997 and 2015. *Geophys. Res. Lett.*, **46**, 7592–7601.
- Yoshida, R., Y. Kajikawa, and H. Ishikawa, 2014: Impact of boreal summer intraseasonal oscillation on environment of tropical cyclone genesis over the western North Pacific. *SOLA*, **10**, 15–18, doi:10.2151/sola.2014-004.
- Wada, A., 2021: Roles of oceanic mesoscale eddy in rapid weakening of typhoons Trami and Kong-Rey in 2018 simulated with a 2-km-mesh atmosphere-wave-ocean coupled model. *J. Meteor. Soc. Japan*, **99**, 1453–1482, doi:10.2151/jmsj.2021-071.
- Wang, B., and J. C. L. Chan, 2002: How strong ENSO events affect tropical storm activity over the western North Pacific. *J. Climate*, **15**, 1643–1658.
- Zhang, W., G. A. Vecchi, H. Murakami, G. Villarini, and L. Jia, 2016: The Pacific meridional mode and the occurrence of tropical cyclones in the western North Pacific. *J. Climate*, **29**, 381–398.

Manuscript received 31 December 2021, accepted 13 March 2022
 SOLA: <https://www.jstage.jst.go.jp/browse/sola/>